Biosensors and Bioelectronics 192 (2021) 113519

Contents lists available at ScienceDirect

Biosensors and Bioelectronics

journal homepage: www.elsevier.com/locate/bios

The role of graphene patterning in field-effect transistor sensors to detect the tau protein for Alzheimer's disease: Simplifying the immobilization process and improving the performance of graphene-based immunosensors

Sun Sang Kwon [a], Dongwoo Kim [b], Mijin Yun [b], Jeong Gon Son [c], Soo Hyun Lee [a,*]

[a] Center for BioMicrosystems, Brain Science Institute, Korea Institute of Science and Technology, Seoul, 02792, South Korea
[b] Department of Nuclear Medicine, Yonsei University College of Medicine, Seoul, 03722, South Korea
[c] Soft Hybrid Materials Research Center, Advanced Materials Research Division, Korea Institute of Science and Technology, Seoul, 02792, South Korea

ARTICLE INFO

Keywords:
Graphene patterning
Field-effect transistor sensor
Immunosensor
Antibody immobilization
Linker-free
Tau protein

ABSTRACT

We report the improvement in the sensing performance of electrolyte-gated graphene field-effect transistor (FET) sensors capable of detecting tau protein through a simplified, linker-free, anti-tau antibody immobilization process. For most of the graphene-based immunosensor, linkers, such as pyrenebutanoic acid, succinimidyl ester (PSE) must be used to the graphene surface, while the other side of linkers serves to capture the antibodies that can specifically interact with the target biomarker. In this study, graphene was patterned into eight different types and linker-free patterned graphene FET sensors were fabricated to verify their detection performance. The linker-free antibody immobilization to patterned graphene exhibited that the antibody was immobilized to the edge defect and had a doping-like behaviors on graphene. As the tau protein concentration in the electrolyte increased from 10 fg/ml to 1 ng/ml, the performances, charge neutral point shift and current change rate of the patterned graphene sensors without linkers were enhanced 2–3 times compared to a pristine graphene sensor with the PSE linker. Moreover, tau protein in the plasma of five Alzheimer's disease patients was measured using a linker-free patterned graphene sensor. It shows a 3–4 times higher current change rate than that of pristine graphene sensor with the PSE linker. Since the antibody is immobilized directly without a linker, a patterned graphene sensor without a linker can operate more sensitively in higher ionic concentration electrolyte.

1. Introduction

The tau proteins, one of the core biomarkers of Alzheimer's disease (AD), are mostly in the cerebrospinal fluid (CSF), and measuring the total levels of tau in the CSF is a good predictor of AD symptoms. The procedures used to extract CSF can cause discomfort or pain in the patient, and some problems can occur, such as headaches due to CSF leakage and nerve damage (Nath et al., 2018), so biomarker detection studies through blood, plasma, and saliva have been conducted to address these issues (Lau et al., 2015). However, the lack of sensitivity due to the low concentration of biomarkers in the blood and higher ionic concentration of blood are the important challenges in measuring the concentration of the tau protein in blood or plasma (Derkus et al., 2016; Yang et al., 2017). Therefore, there is a need for a method that can detect tau protein accurately in blood or plasma.

Graphene, two-dimensional carbon allotropes that consist of sp^2 hybridization, shows excellent electrical conductivity, high carrier mobility (Du et al., 2008; Rana et al., 2014), and a low *1/f* noise level (Cheng et al., 2010). Due to its large surface-to-volume ratio, good chemical/biological stability, and good biocompatibility (Kang et al., 2016), graphene is considered a good material for use as sensors, and it has been studied extensively for detecting chemical and biological changes in electrolytes or in ambient air (Pumera, 2011; Lee et al., 2015). When the target analyte species or the concentration in the electrolyte is changed, it can be detected by the change in the electrical conductance of graphene field-effect transistor (FET) caused by the adsorption of target analytes near the surface of the graphene (Huang et al., 2011; An et al., 2013).

For this operation, receptors, such as antibodies, peptides, and aptamers, must be attached to the surface of the graphene and then the specific target analyte should be captured near the surface of the graphene. However, since graphene is an atomically flat and inert material

* Corresponding author.
E-mail address: shleekist@kist.re.kr (S.H. Lee).

https://doi.org/10.1016/j.bios.2021.113519
Received 26 May 2021; Received in revised form 14 July 2021; Accepted 16 July 2021
Available online 24 July 2021

composed of only sp^2 hybridized bonds of carbon, only very few functional groups, such as pyrene, can be attached to the basal plane of graphene through π-π interactions. Therefore, pyrene-functionalized linkers, such as pyrenebutanoic acid, succinimidyl ester, or pyrenebutyric acid (e.g., PSE, PBASE) were used to immobilize the receptors on the surface of the graphene (Fig. 1a) (Wang et al., 2015; Gao et al., 2016). To further improve the performance of the sensor, studies have been published in which defects were generated in the graphene through graphene patterning or treatment with O_2 plasma (Tan et al., 2013; Yuan et al., 2019). The generated point or line defects are more suitable for chemical reactions because they are O-group functionalized and exposed directly to the ions/molecules in electrolyte (Sharma et al., 2010; Yuan et al., 2013). However, some parameters of the patterned graphene were not taken into account, such as the width and shape of the channel, i.e., whether it was a nanoribbon or a mesh, and the process of generating defects was determined arbitrarily for each experiment.

In this study, we investigated whether the performance of a patterned graphene sensor can be improved by controlling the graphene patterning parameters and the immobilization process without a linker (Fig. 1b). Nine different types of graphene sensors were prepared, and anti-tau antibodies were immobilized with and without the PSE linker. It was confirmed that the performance of the sensor, in particular the current change rate, was increased to two times that of the non-patterned graphene sensor with the PSE linker through graphene patterning, and it also works at the low concentration of 10 fg/ml. In addition, the patterned graphene sensors without linkers have the advantage of operating in higher ionic strength electrolytes, such as serum or plasma, because the anti-tau antibody binds directly to the oxidative edges of the graphene (Jia et al., 2011).

2. Experimental

2.1. Graphene patterning process and fabrication of the graphene field-effect transistor

The source and drain electrodes were defined using AZ 9260 as photoresist (PR) and photolithography equipment (Karl Suss) on 285 nm SiO_2/Si substrate. The AZ 9260 was coated using a spin coater at 2000 rpm for 30 s and progressively prebaked at 95 °C for 5 min and 110 °C for 8 min. The prepared PR layer was exposed to 1580 mJ/cm^2 and developed with AZ 400 K 1:3 developer for 13 min. After the lithography process, 15 nm titanium adhesive layer and 85 nm thick platinum was deposited on pre-patterned substrate by RF sputter. For the lift-off process, electrode deposited substrate was immersed in acetone for 30 min and rinsing with 2-propanol (IPA). A graphene film was grown by chemical vapor deposition (CVD) process on 25 μm thick copper (Cu) foil (Alfa Aesar, #10950), using 40 sccm hydrogen and 100 sccm methane as a carrier gas and carbon source, respectively, at 1000 °C for 15 min. The graphene film on the Cu foil was coated with a poly (methyl methacrylate) (PMMA) (Micro chem, 950 PMMA A2) layer to minimize the mechanical fracture during the Cu etching. The PMMA/graphene/Cu foil layer was floated on a 0.05 M ammonium persulfate solution (Sigma Aldrich, #248614) to remove the underlying Cu foil layer. After the Cu etching, the lower surface of the freestanding PMMA/graphene layer was washed at least twice with deionized water and transferred onto the electrode defined substrate and dry with ambient air. The PMMA layer was removed with acetone for 2 min and rinsed with IPA for 2 min and rapid thermal annealing (RTA) at 300 °C for 30 min to remove any other polymer residues.

The graphene was patterned with photolithography process using AZ GXR-601 14cp as PR. The AZ GXR-601 14 cp was coated using a spin coater at 4500 rpm for 40 s and prebaked at 95 °C for 90 s. The prepared PR layer was exposed to 32 mJ/cm^2, post exposure baked at 110 °C for 90 s and developed with AZ MIF 300 developer. After the PR patterning process, opened pattern area of graphene was etched with O_2 plasma equipment (500 mTorr, 50 kHz frequency, 100 W for 40 s) and immersed in acetone for 30 min and rinsing with IPA to remove the remain photoresist layer.

2.2. Immobilization of anti-tau antibody on the graphene with and without a linker

To immobilize the anti-tau antibody onto the surface of the graphene, the poly (dimethylsiloxane) (PDMS) (Dow corning, Sylgard 184) block with 2 × 3 mm^2 opened window was clamped on to the graphene FET device to prevent the direct immersion of source and drain

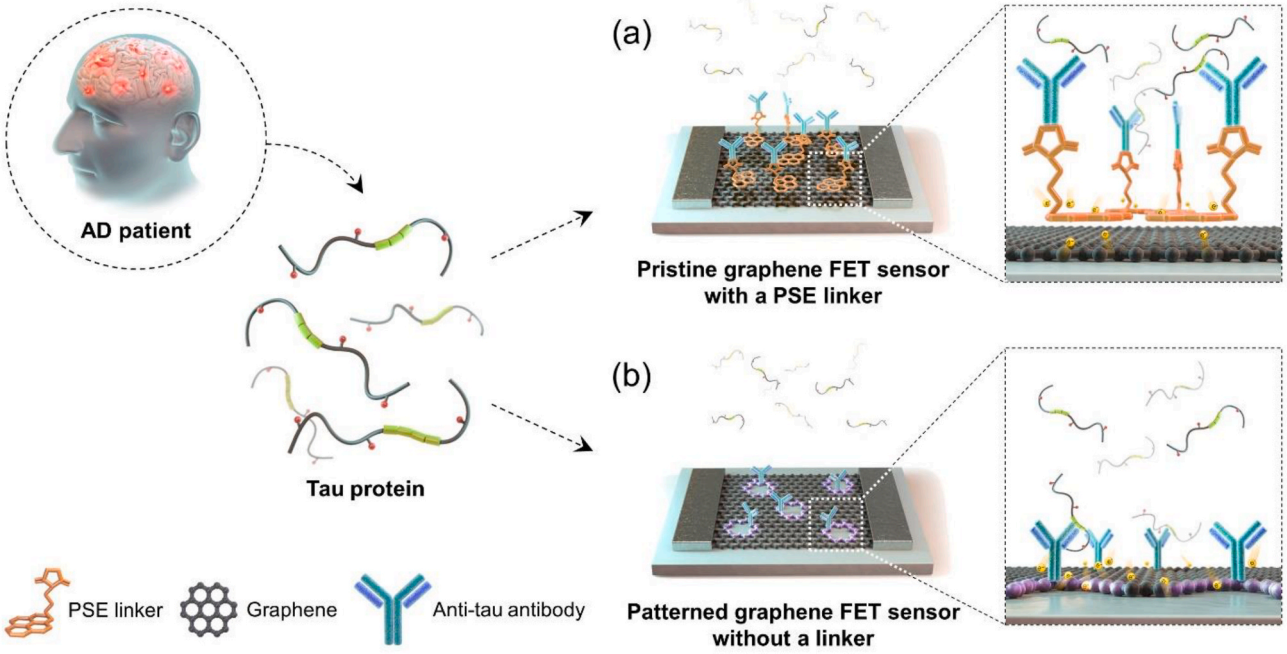

Fig. 1. Schematic images of the electrolyte-gated, graphene-based FET tau sensor; (a, b) Representative schematic images of antibody immobilized on (a) pristine graphene with the PSE linker and (b) patterned graphene without a linker.

electrodes to the solutions. The exposed pristine and patterned graphene were then incubated with 5 mM PSE (Anaspec, AS-81238) at room temperature for 1 h and rinsed with methanol and 1X phosphate-buffered saline (PBS) (Welgene, ML 008–01). After the linker functionalization, the pristine and patterned graphene with the PSE linker on its surface were incubated with the 2 μg/ml anti-tau antibody solution (Abcam, ab64193) overnight at 4 °C. Just before the measurement, anti-tau antibody solution incubated device was rinsed with PBS and incubated with 3 % bovine serum albumin (BSA) (Sigma Aldrich, A2153), to prevent non-specific binding for 1 h at room temperature and then rinsed with PBS again. The anti-tau antibody immobilization without the linker devices skips the PSE linker functionalization process but undergo same anti-tau antibody immobilization and BSA blocking process.

2.3. Measurement setup for electrolyte-gated graphene-based immunosensors

To measure the electrical properties of electrolyte-gated graphene FET device, semiconductor device analyzer (Agilent Technologies, B1500A) was used as three electrode measurement system. As a reference gate electrode, silver/silver chloride (Ag/AgCl) was prepared by dipping Ag wire in a solution rich in chlorine ions overnight and inserted into the PDMS well during the measurement. The source-drain bias (V_{sd}) was 500 mV and the V_g was swept from −0.5 V to 1.5 V with 0.01 V step. The recombinant tau protein samples (Sigma Aldrich, T0576) were prepared in PBS which concentrations were 10 fg/ml, 100 fg/ml, 1 pg/ml, 10 pg/ml, 100 pg/ml, and 1 ng/ml, respectively. All recombinant tau protein samples were stored at 4 °C before the measurement and at every solution exchange step, the sensor surfaces were gently rinsed with PBS. When the solution has been exchanged, the device was incubated for 3 min and then characteristic source-drain current versus gate voltage (I_{sd}-V_g) transfer curve measurements were conducted.

2.4. Comparison of the performance of the graphene-based immunosensors through detection of tau protein in clinical samples

To compare the detection performance of the graphene sensor with the PSE linker and the patterned graphene sensor without a linker, artificial serum samples and clinical samples were measured with the graphene sensors. Artificial serum samples were prepared by 20-fold dilutions of recombinant tau protein at concentrations of 20 pg/ml, 200 pg/ml, 2 ng/ml, and 20 ng/ml using commercialized human serum (Sigma Aldrich, H4522) to obtain 1 pg/ml, 10 pg/ml, 100 pg/ml, and 1 ng/ml tau protein concentrations. Clinical plasma samples were collected from two normal control (NC) and five different AD patients and stored at −80 °C for use. This study was approved by the institutional review board (IRB), and written informed consent was obtained from all patients (4-2019-0935). The same measurement setup as the recombinant tau protein was used, but commercialized human serum was used instead of PBS to measure a reference I_{sd}-V_g transfer curve that did not contain the tau protein. All clinical samples were thawed at 4 °C for about 30 min prior to measurement. For each device, a total of two characteristic I_{sd}-V_g transfer curves, reference and clinical samples were measured sequentially after 3 min incubation time. Human tau (total) concentration was also measured using an ELISA kit (Invitrogen, KHB0041) to verify the performance of the graphene-based immunosensor performance.

3. Results and discussion

3.1. Preparation of nine different types of graphene

Nine different types of graphene, consisting of four different types of grid-patterned graphene, four different types of round hole mesh patterned graphene with oxidative edge defects, and pristine graphene without edge defects, were prepared and fabricated into FETs to test their performance. In Figure S1, both grid and mesh structures have four different types of structural parameters, i.e., 150/100 μm, 300/500 μm, 150/50 μm, and 30/10 μm, as graphene inter-channel spacing/channel widths, respectively. Table S1 shows the calculated porosity and the density of the edge defects for each pattern. (See supplementary information for details.)

3.2. Shift of the transfer curve of the graphene FET during the antibody immobilization process

To see the anti-tau antibody immobilized on the pristine graphene with and without PSE linker functionalization and patterned graphene with and without PSE linker functionalization, the I_{sd}-V_g transfer curves were measured during the anti-tau antibody immobilization process. All of the kinds of graphene FETs in the I_{sd}-V_g plot exhibited a V-shaped curve since the graphene has ambipolar character (Figure S2). The value of the voltage at the lowest current in the transfer curve is referred to as the Dirac point or charge neutral point (V_{CNP}).

The V_{CNP} values in Fig. 2a were extracted from each of the transfer curves in Figures S2a-c, and the 150/50 patterned graphene was chosen because it showed the highest V_{CNP} shift as the tau protein concentration increased in the electrolyte. After the functionalization of the PSE linker, the transfer curves of graphene FETs shifted in the positive direction by about 150 mV. This was due to the negatively charged aromatic ring parts of the PSE linker that were adsorbed on the surface of the graphene (Hao et al., 2020). After the antibody immobilization step, the transfer curve of pristine graphene FET with a PSE linker shifts by 32 mV, whereas 150/50 patterned graphene FETs with PSE linkers shifted about 20 mV. The larger shift in the pristine graphene FET transfer curve is because the surface area of graphene is larger than that of the patterned graphene FETs about 166 %, so it is affected by more immobilized anti-tau antibodies.

Anti-tau antibody immobilization without a linker has a different trend of the shift in the transfer curve than antibody immobilization with the PSE linker. The transfer curve of the pristine graphene FET without a linker hardly was shifted at all after the anti-tau antibody immobilization step. Since anti-tau antibody immobilization without a linker rarely occurs on the surface of the graphene, the pristine graphene FET without a linker did not exhibit shifts in the transfer curve after the antibody immobilization step. However, in the case of the 150/50 patterned graphene FETs without a linker, the V_{CNP} shifted in the positive direction by 40 mV after the anti-tau antibody immobilization process (Fig. 2b). Except for the pristine graphene FET without a linker, the V_{CNP} shifted from 5 to 10 mV in the negative direction after the BSA blocking process.

The shift of the transfer curve in the opposite direction based on the presence or absence of the functionalization of the PSE linker was assumed to be due to the difference in the way the anti-tau antibody is immobilized to graphene. In terms of the electrostatic gating mechanism, the negative shift of the transfer curve after antibody immobilization in the graphene FETs with PSE linkers means that the total charge on the surface of the graphene increased through the anti-tau antibody immobilization process. However, in the patterned graphene FETs without linkers, the transfer curve shifts in the positive direction after the anti-tau antibody immobilization cannot be explained reasonably by the electrostatic gating mechanism. The defect doping mechanism, in which the antibody binds directly to the oxidized graphene edge defects, is one of the candidates for explaining this anomaly, and further surface analyses confirm this assumption (Figures S3 and S4). In this case, the anti-tau antibody is thought to act as a hole donor by binding directly to the edge defects of the patterned graphene FETs without linkers (Brenner et al., 2012).

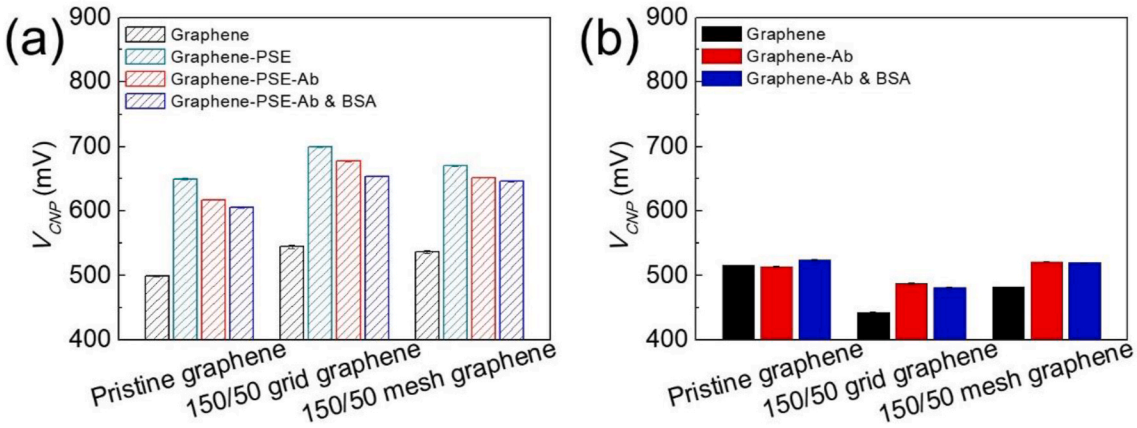

Fig. 2. The V_{CNP} shift of the graphene FETs during the antibody immobilization process: (a) The V_{CNP} values of the anti-tau antibody immobilized with the PSE linker on the graphene FETs; (b) The V_{CNP} values of the anti-tau antibody immobilized without linkers on the graphene FETs.

3.3. Characteristic transfer curves of the graphene FET sensor

To evaluate the performance of the sensor, the I_{sd}-V_g transfer curve of the graphene FET sensors were measured and the V_{CNP} shift or by the change in the current due to a change in the concentration of the target analyte were compared.

In Fig. 3a, the transfer curves and V_{CNP} of a conventional graphene sensor, with the antibody immobilized with the PSE linker to pristine graphene, was located at 620 mV when the electrolyte did not contain tau protein. The V_{CNP} began to shift at 619.5 mV when the electrolyte contained a tau protein concentration of 10 fg/ml, and each time the solution exchanged with a ten-fold increase in the concentration of tau protein, the transfer curve and V_{CNP} shifted about 8.5 mV in the negative direction. In Figures S5a-c, the V_{CNP} of the patterned graphene sensors with the PSE linkers also shifted in the negative direction with a ten-fold increase in the tau protein concentration, but the degrees of change decreased to 3.2 mV and 3.9 mV, respectively. The reduction of the sensor's performance for patterned graphene sensors with the PSE linker were due to the reduction in the surface area of graphene (Kwon et al., 2017).

The transfer curves and V_{CNP} shift of the 'linker-free' graphene sensors were also plotted in Figures S5d, 3b, 3c, and S6. The transfer curve and V_{CNP} of the patterned graphene sensors without linkers also shifted negatively as the concentration of tau protein in the solution increased, but the degree of shift depended on the size of the graphene pattern. The pristine graphene sensor without a linker exhibited negligible change since the antibody was rarely adsorbed to the graphene surface (Figure S5d).

In Fig. 3d and e, for the patterning parameters of 150/50 (blue) and 30/10 patterned graphene without a linker (magenta), V_{CNP} changes more significantly with tau protein injection (10 fg/ml) and increasing concentration. However, under different patterning conditions, such as 150/100 and 300/50 patterned graphene without the linker, the change in V_{CNP} and its performance appear to be similar to that of a pristine graphene sensor with the PSE linker. Fig. 3f shows the performance of the graphene sensors according to the density of the edge defects. The performance improved if the density of the edge defects was greater than 15 mm^{-1}, but it was obvious that the performance decreased compared

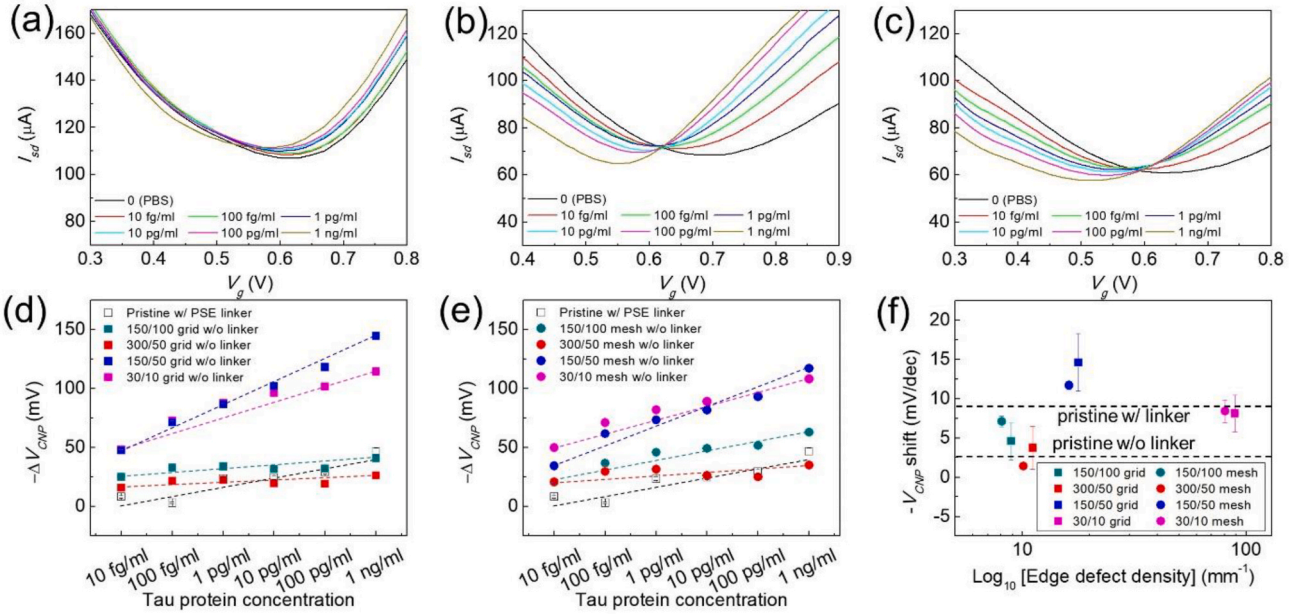

Fig. 3. The transfer curves and the V_{CNP} shift of the graphene sensors: (a–c) The curves of (a) the pristine graphene sensor with the PSE linker, (b) the 150/50 grid-patterned, and (c) the 150/50 mesh-patterned graphene sensors without linkers; (d, e) The tau concentration-dependent V_{CNP} values of (d) the grid-patterned and (e) the mesh-patterned graphene sensors without linkers; (f) The density of the edge defect-dependent V_{CNP} shift of the patterned graphene sensors without linkers.

to the pristine graphene sensor with the PSE linker when the density of the edge defects was as low as 10 mm^{-1}. Around 8 mm^{-1} the edge defect density with a 150/100 patterned graphene exhibited lower changes in V_{CNP} than a pristine graphene sensor with the PSE linker because the density of the immobilized antibodies decreased due to the low density of the defects. However, the lowest V_{CNP} change in the edge defect density around 10 mm^{-1}, the 300/50 patterned graphene, appears to be due to the degradation of graphene due to excessive patterning, and a similar deterioration appeared in graphene functionalization via treatment with O_2 plasma (Yuan et al., 2019).

3.4. Current change rate of the graphene FET sensor

To further investigate the performance of the sensor through graphene patterning and linker-free immobilization, the current change rate is calculated from the characteristics transfer curves of each graphene sensors as follows:

$$Currentchangerate = \frac{\Delta I}{I_{PBS}} = \frac{I_{Con.} - I_{PBS}}{I_{PBS}} \quad (1)$$

where $I_{Con.}$ Is the value of the current measured with a specific tau protein concentration, and I_{PBS} is the current measured with PBS at the same V_g of 750 mV (Figure S7).

In Fig. 4a and b, the current change rate of the pristine graphene sensor with the PSE linker (black, open square) starts at 4.09 % when the tau protein concentration in the electrolyte is 10 fg/ml, and it is increased by about 3 % as the concentration increased ten-fold. However, the patterned graphene sensors without linkers show the current change rates start at about 11 % or more when the tau protein concentration is 10 fg/ml, and they increased by 4.09 % as the concentration increased by a factor of 10. Fig. 4c shows that the increase of in the rate of change of the current is proportional to the density of edge defects, and for a 30/10 patterned graphene sensors without linkers with the highest edge density, the performance improves to about 8 %/dec. It is presumed that the reason for the improvement in the performance in proportion to the density of the edge defect is because the amount of antibody to be immobilized increases as the edge defect density increases. Note that the 150/100 patterned graphene sensors without linkers performed better on the slope of the current change rate even though the result of the V_{CNP} shift was worse than that of the pristine graphene sensor with the PSE linker (Fig. 3f). According to the concept of defect doping, even if a small amount of the anti-tau antibody is bound, the electron or the hole generated as a result of the antigen-antibody reaction is transferred more easily to the graphene, resulting in enhancing the rate at which the current changes. The 300/50 patterned graphene sensors without linkers are the only exceptional patterns, and, as mentioned above, the large pattern size compared to the width of the channel and the reduced density of immobilized antibodies appear to exacerbate the performance of the sensor.

To clarify the reason for the improvement in the performance of the sensor, the transconductance (g_m) was calculated from each of the characteristic transfer curves. Figure S8 shows that the graphene sensors with the PSE linkers hardly changed the g_m even when the concentration of the tau protein increased. In contrast, the g_m of the patterned graphene sensors without linkers increased at a V_g of 750 mV as the concentration of the tau protein in the electrolyte increased from 10 fg/ml to 1 ng/ml, except for the 300/50 patterned graphene sensors that did not have linkers (Figure S9).

The value of g_m is calculated from the charge transport characteristics as follows (Xu et al., 2011):

$$g_m = \frac{dI_{sd}}{dV_g} = \mu C_T \frac{W}{L_g} V_{sd} \quad (2)$$

where W and L_g are the width and length of the graphene channel, respectively, V_{sd} is the source-drain bias (500 mV), μ is the carrier mobility of graphene, and C_T is the total gate capacitance. From equation (2), W, L_g, and V_{sd} are constant, and the value of C_T will not change because there is no significant effect on the capacitance of the double layer in the tau protein concentration range under measurement conditions. Therefore, the change in the value of g_m with the increasing concentration of tau protein can be expected mainly due to the increase in μ, and it can occur through electron or hole transfer of graphene (Rajiv et al., 2012; Cao et al., 2020). From this, it can be assumed that an anti-tau antibody that binds directly to the edge defects of graphene without a linker can improve the detection performance by injecting electrons or holes directly into the graphene as well as using the commonly known electrostatic gating through reaction with tau protein (Scheme S2).

Another feature in Fig. 4a and b is that the grid-patterned graphene sensors without linkers have a steeper slope, but it also has a higher deviation of the current change rate than the mesh-patterned graphene sensors without linkers due to the change in the concentration of tau protein. The edge defects of graphene have a significant influence on the chemical reactivity depending on the edge chirality (Kim et al., 2018), and the grid-patterned graphene in which the edge defects are formed perpendicular to each other can show a large difference in edge chirality for each device. However, in the case of mesh-patterned graphene, the edge chirality of the round-shaped edges can be evenly distributed compared to the grid-patterned graphene, so the immobilized antibody has a relatively uniform effect, and the performance of the sensor appears to be more reliable (Yang et al., 2014).

3.5. Detection of tau protein from clinical samples

The detection performance of the patterned graphene sensor without a linker was tested using artificial serum samples and clinical samples

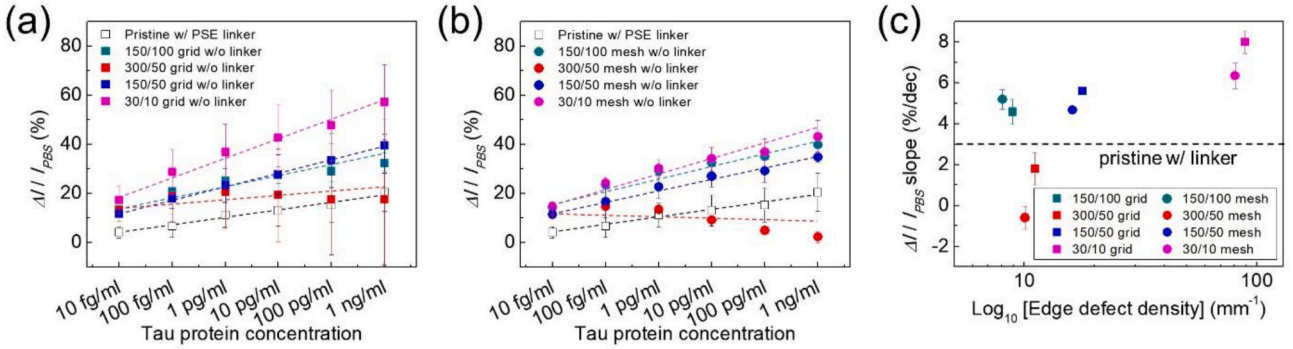

Fig. 4. The change in the current rate comparison of the graphene sensors without linkers: (a, b) The concentration of the tau protein-dependent current change rates at $V_g = 0.75$ V of (a) the grid-patterned graphene and (b) the mesh-patterned graphene sensors without linkers; (c) Density of the edge defects-dependent current change rates of the patterned graphene sensors without linkers.

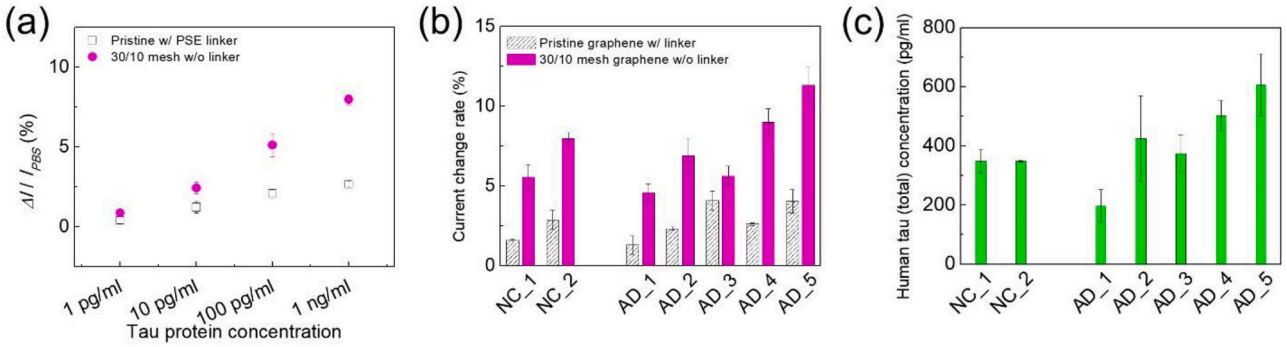

Fig. 5. Comparison of the performance of the sensor through artificial serum samples and clinical samples: (a) The concentration of the tau protein in artificial serum-dependent current change rates; (b) The current change rate measured with (black) the pristine graphene sensor with the PSE linker and (magenta) the 30/10 mesh-patterned graphene sensor without a linker using clinical samples; (c) Human tau protein concentration measured with ELISA kit.

(Fig. 5). The 30/10 mesh-patterned graphene sensor without a linker was chosen because it had the best performance with stable results in this study. Each clinical sample was collected from two different NC and five different AD patients, and the performance of the sensor was confirmed with additional enzyme-linked immunosorbent assay (ELISA) measurements.

In Fig. 5a, the current change rate of the pristine graphene sensor with the PSE linker starts under 1 % when the tau protein concentration in the commercialized serum is 1 pg/ml, and it is increased by about 0.7 % as the concentration increased by a factor of 10. The 30/10 mesh patterned graphene sensor without a linker also shows the current change rate starts under 1 % when the tau protein concentration is 1 pg/ml, but increased by 2.5 % as the concentration increased ten-fold.

In Fig. 5b, the pristine graphene sensor with the PSE linker exhibits a 1.3–4.0 % rate of change in the current for each clinical sample. In contrast, the rate of change in the current of the 30/10 mesh-patterned graphene sensor without a linker was 4.5–11.3 % for each clinical sample, which is larger than that of the pristine graphene sensor with the PSE linker. Note that the current change rate of the 30/10 mesh-patterned graphene FET sensor without a linker tended to be similar to the total human tau concentration measured by ELISA (Fig. 5c).

The overall weak signal of a pristine graphene sensor with the PSE linker than a patterned graphene sensor without a linker is related to the sensing mechanism and the ion concentration in the electrolyte. In a solution with high ionic concentrations, such as human plasma (Covington et al., 1975), the Debye length of the graphene interface is shortened, reducing the effect of electrostatic gating that detect electrical charges on the surface (Kulkarni et al., 2012; Gao et al., 2015).

However, the 30/10 mesh-patterned graphene sensor without a linker proposed in this study appears to have the anti-tau antibody bound directly to graphene. This direct binding is thought to be less affected by Debye screening as the charge is transferred directly to the graphene through the interaction between the anti-tau antibody and the tau protein. As a result, the electrical properties of graphene respond more directly to the interaction between the tau protein and the anti-tau antibody, and it shows better performance and greater accuracy than a conventional graphene sensor with the PSE linker.

4. Conclusions

We performed graphene patterning to simplify the antibody immobilization process and improve the performance of the graphene-based, electrolyte-gated FET sensor. In the conventional method, the antibody is immobilized with the PSE linker, and the antibody is adsorbed onto the surface of the graphene through indirect π-π interactions. While, when edge defects are formed through graphene patterning, antibodies are bonded directly through oxidized graphene edges. Through this direct binding, the charge changed by the interaction of the tau protein and the anti-tau antibody was transferred directly to graphene, and the electrical property, especially the current change rate, was improved in proportion to the increase in the density of the edge defects. Another advantage of simplifying the antibody immobilization process through graphene patterning is the improved performance of the sensor when used in physiological measurement conditions. In electrolytes with high ionic strength, such as blood and plasma, the Debye length that is inversely proportional to ion concentration is known to degrade the performance of conventional graphene FET sensors that operate with electrostatic gating effect. However, when the antibody is bound directly to the graphene through graphene patterning, a kind of defect doping operation that transfers charge directly from the antibody irrespective of the Debye length allows improved and accurate measurements, even in electrolytes that have high ionic strength. In this study, the performance of the graphene-based immunosensor was improved through graphene patterning, but it is necessary to consider whether the performance can be improved further as the size of the pattern is reduced to the nanoscale (Oh et al., 2017). In addition, even if the conventional electrostatic gating effect and the defect doping appear at the same time, as we have claimed, the effect and weight of both are still uncertain, so more studies are needed.

CRediT authorship contribution statement

Sun Sang Kwon: Investigation, Visualization, Writing – original draft. **Dongwoo Kim:** Clinical sample collection, Clinical diagnosis of the AD patient, and. **Mijin Yun:** Clinical sample collection, Clinical diagnosis of the AD patient. **Jeong Gon Son:** Writing – review & editing, Providing graphene growth conditions and CVD equipment, writing-review. **Soo Hyun Lee:** Supervision, Writing – review & editing, Project administration, Funding acquisition.

Declaration of competing interest

The authors declare that they have no known competing financial interests or personal relationships that could have appeared to influence the work reported in this paper.

Acknowledgments

This research is partially funded by the Brain Research Program through the National Research Foundation of Korea (NRF-2016M3C7A1913845, NRF-2018M3C7A1056896), the National Research Council of Science & Technology (No. CRC-15-04-KIST) funded by the Ministry of Science, ICT & Future Planning (MSIP), and the Korea Health Technology R&D Project through the Korea Health Industry Development Institute (KHIDI) and Korea Dementia Research Center (KDRC), funded by the Ministry of Health & Welfare and Ministry

of Science and ICT, Republic of Korea (grant number: HU20C0164). S.S. K. thanks the support by the National Research Foundation of Korea (NRF-2020R1A6A3A01100437).

Appendix A. Supplementary data

Supplementary data to this article can be found online at https://doi.org/10.1016/j.bios.2021.113519.

References

An, J.H., Park, S.J., Kwon, O.S., Bae, J., Jang, J., 2013. ACS Nano 7 (12), 10563–10571.
Brenner, K., Yang, Y.X., Murali, R., 2012. Carbon 50 (2), 637–645.
Cao, Y.Y., Huang, L.L., Diao, D.F., 2020. Adv.Mater.Interfac.
Cheng, Z.G., Li, Q., Li, Z.J., Zhou, Q.Y., Fang, Y., 2010. Nano Lett. 10 (5), 1864–1868.
Covington, A.K., Robinson, R.A., 1975. Anal. Chim. Acta 78 (1), 219–223.
Derkus, B., Ozkan, M., Emregul, K.C., Emregul, E., 2016. RSC Adv. 6 (1), 281–289.
Du, X., Skachko, I., Barker, A., Andrei, E.Y., 2008. Nat. Nanotechnol. 3 (8), 491–495.
Gao, N., Gao, T., Yang, X., Dai, X.C., Zhou, W., Zhang, A.Q., Lieber, C.M., 2016. P.Natl. Acad. Sci. U.S.A. 113 (51), 14633–14638.
Gao, N., Zhou, W., Jiang, X., Hong, G., Fu, T.-M., Lieber, C.M., 2015. Nano Lett. 15 (3), 2143–2148.
Hao, Z., Pan, Y.L., Huang, C., Wang, Z.R., Lin, Q., Zhao, X.Z., Liu, S.Q., 2020. ACS Sens. 5 (8), 2503–2513.
Huang, Y.X., Dong, X.C., Liu, Y.X., Li, L.J., Chen, P., 2011. J. Mater. Chem. 21 (33), 12358–12362.
Jia, X., Campos-Delgado, J., Terrones, M., Meunier, V., Dresselhaus, M.S., 2011. Nanoscale 3, 86–95.
Kang, P.Y., Wang, M.C., Nam, S., 2016. Microelectron. Eng. 161, 18–35.
Kim, J., Lee, N., Min, Y.H., Noh, S., Kim, N.-K., Jung, S., Joo, M., Yamada, Y., 2018. ACS Omega 3 (12), 11789–117796.
Kulkarni, G.S., Zhong, Z., 2012. Nano Lett. 12 (2), 719–723.
Kwon, S.S., Shin, J.H., Choi, J., Nam, S., Park, W.I., 2017. ACS Appl. Mater. Interfaces 9 (16), 14216–14221.
Lau, H.C., Lee, I.K., Ko, P.W., Lee, H.W., Huh, J.S., Cho, W.J., Lim, J.O., 2015. PloS One 10 (2).
Lee, M.H., Kim, B.J., Lee, K.H., Shin, I.S., Huh, W., Cho, J.H., Kang, M.S., 2015. Nanoscale 7 (17), 7540–7544.
Nath, S., Koziarz, A., Badhiwala, J.H., Alhazzani, W., Jaeschke, R., Sharma, S., Banfield, L., Shoamanesh, A., Singh, S., Nassiri, F., Oczkowski, W., Belley-Cote, E., Truant, R., Reddy, K., Meade, M.O., Farrokhyar, F., Bala, M.M., Alshamsi, F., Krag, M., Etxeandia-Ikobaltzeta, I., Kunz, R., Nishida, O., Matouk, C., Selim, M., Rhodes, A., Hawryluk, G., Almenawer, S.A., 2018. Lancet 391 (10126), 1197–1204.
Oh, J., Yoo, H., Choi, J., Kim, J.Y., Lee, D.S., Kim, M.J., Lee, J.-C., Kim, W.N., Grossman, J.C., Park, J.H., Lee, S.-S., Kim, H., Son, J.G., 2017. Nanomater. Energy 35, 26–35.
Pumera, M., 2011. Mater. Today 14 (7–8), 308–315.
Rajiv, S., Sujata, P., Bala, J.S., 2012. J. Semiconduct. 33, 024001.
Rana, K., Singh, J., Ahn, J.H., 2014. J. Mater. Chem. C 2 (15), 2646–2656.
Sharma, R., Baik, J.H., Perera, C.J., Strano, M.S., 2010. Nano Lett. 10 (2), 398–405.
Tan, X.B., Chuang, H.J., Lin, M.W., Zhou, Z.X., Cheng, M.M.C., 2013. J. Phys. Chem. C 117 (51), 27155–27160.
Wang, C., Kim, J., Zhu, Y.B., Yang, J.Y., Lee, G.H., Lee, S., Yu, J., Pei, R.J., Liu, G.H., Nuckolls, C., Hone, J., Lin, Q., 2015. Biosens. Bioelectron. 71, 222–229.
Xu, H.L., Zhang, Z.Y., Xu, H.T., Wang, Z.X., Wang, S., Peng, L.M., 2011. ACS Nano 5 (6), 5031–5037.
Yang, J., Ma, M.Z., Li, L.J., Zhang, Y.F., Huang, W., Dong, X., 2014. Nanoscale 6 (22), 13301–13313.
Yang, S.Y., Chiu, M.J., Chen, T.F., Lin, C.H., Jeng, J.S., Tang, S.C., Lee, Y.F., Yang, C.C., Liu, B.H., Chen, H.H., Wu, C.C., 2017. Sci Rep-Uk 7.
Yuan, Q.L., Wu, S.D., Ye, C., Liu, X.Q., Gao, J.Y., Cui, N.Y., Guo, P., Lai, G.S., Wei, Q.P., Yang, M.H., Su, W.T., Li, H., Jiang, N., Fu, L., Dai, D., Lin, C.T., Chee, K.W.A., 2019. Sensor. Actuator. B Chem. 285, 333–340.
Yuan, W.J., Zhou, Y., Li, Y.R., Li, C., Peng, H.L., Zhang, J., Liu, Z.F., Dai, L.M., Shi, G.Q., 2013. Sci Rep-Uk 3.